Catalysis
Science & Technology

RSC Publishing

PAPER

View Article Online
View Journal | View Issue

Cite this: *Catal. Sci. Technol.*, 2013, **3**, 1634

Structural changes in FeMFI during its activation for the direct ammoxidation of propane

Kateřina Raabová,*[a] Eva Bad'urová,[a] Roman Bulánek,[a] Pierre Eloy[b] and Eric M. Gaigneaux[b]

Received 16th January 2013,
Accepted 7th April 2013

DOI: 10.1039/c3cy00040k

www.rsc.org/catalysis

Various characterization techniques, including UV-Vis, FTIR, EPR and XPS, were used for the description of structural changes in Fe-silicalite with low concentration of iron, which was activated using different methods (by conventional hydrothermal pretreatment at 600 °C and by treatment in the diluted flow of ammonia and propane in helium at 540 °C). Activated Fe-silicalite was subsequently used as a catalyst for the direct ammoxidation of propane. It has been shown that the studied methods of activation lead to materials with different catalytic behavior (activation in the flow of ammonia and propane resulting in the more active and selective catalytic materials). Results from the catalytic test are further discussed together with the results from the characterization of activated samples.

1. Introduction

Isomorphous substitution of a small fraction of Si^{4+} by Fe^{3+} in the zeolite with MFI structure leads to Fe-silicalite. This material together with Fe-ZSM-5 is known to show catalytic activity in a number of chemical processes. Reactions catalyzed by these materials include (i) isomerization and oxidative dehydrogenation of alkanes,[1–3] (ii) selective oxidation of benzene to phenol using N_2O as the oxidant,[4–9] (iii) reduction of NO_x and N_2O with hydrocarbons (HC-SCR) or ammonia (NH_3-SCR),[10–19] direct N_2O decomposition[19–22] and also (iv) direct ammoxidation of propane over differently activated Fe-silicalite in the presence of O_2 or O_2/N_2O as the oxidants.[23–25]

For most of these reactions, the catalytic activity is thought to be related to extraframework iron species (iron oxides or oxohydroxide aggregates) formed by Fe extraction during the post-synthesis thermal treatments[1,2,7,8,10–12,16,19,20,23] and acting either independently or in synergy with protonic $\equiv$Fe(OH)Si$\equiv$ (Brønsted acid) sites.[3,5,11,13,14,17,19,24,25] Post-synthesis thermal treatments can be done either by calcination at high temperatures in air or by treatment in a flow of inert gas (or in a vacuum), but also in water vapor.[22] High temperature treatments of isomorphously substituted zeolites induce the removal of Fe^{3+} from the framework to extraframework positions, with subsequent migration and grafting. The process is highly dependent upon the presence of H_2O impurities in the channels, which are known to favor both hydrolysis of SiOSi, SiOAl, SiOFe and FeOFe bridges (with the formation of hydroxylated sites suitable for anchoring of migrating species) and clustering of extraframework species. It is also concluded that the final (active) state of the catalyst is completely different from that of the starting material.[27] Several research groups have investigated the structure–activity relationship of Fe-ZSM-5, particularly the effect of the synthesis procedure on the nature and distribution of iron species and the associated catalytic performance.[11,13,20]

Recently we reported on the study of the effect of Fe-silicalite pretreatment in the diluted stream of ammonia and propane (so called gas-reduction nitridation – GRN)[25] and also on the activation of the same material in the concentrated ammonia at high temperatures.[26] In both cases we found out that these pretreatments led to interesting catalytic properties, which, when compared to other catalysts studied for the ammoxidation of propane, were quite remarkable mainly considering their productivity. In the case of activation of Fe-silicalite in the concentrated ammonia we confirmed the insertion of nitrogen into the zeolite structure by means of FTIR spectroscopy and we described the effect of the nitridation temperature on the formation of nitrided species (either Si–NH–Si, or Si–NH_2 species). In this work we continue studying the catalytic properties of Fe-silicalite pretreated by both GRN and hydrothermal pretreatment as a reference conventional method but in this article the main attention is focused on the spectroscopic characterization (by means of EPR, UV-Vis, FTIR and XPS spectroscopy)

[a] *Department of Physical Chemistry, Faculty of Chemical Technology, University of Pardubice, Pardubice, Studentska 573, 53210, Czech Republic. E-mail: Katerina.Raabova@upce.cz; Fax: +420 466 037 068; Tel: +420 466 037 052*

[b] *Institute of Condensed Matter and Nanoscience – MOlecules, Solids and reactiviTy (IMCN/MOST), Université catholique de Louvain. Croix du Sud 2 box L7.05.17, 1348 Louvain-La-Neuve, Belgium*

of activated materials, which was not discussed in the paper published previously.

2. Experimental

2.1 Preparation of the catalyst and its activation

Fe-silicalite (FeS) catalyst with Fe concentration of 4700 ppm introduced during zeolite synthesis was investigated. Fe-silicalite was prepared using hydrothermal synthesis introduced earlier.[26] Four different pretreatments of Fe-silicalite were investigated (a) a fresh catalyst calcined for 3 hours at 470 °C in a flow of oxygen (denoted FeS-calc3) at a flow rate of 25 ml min^{-1} (b) treatment for 5 hours in the 5 vol% of propane and 5 vol% of ammonia mixture in the flow of He at a total flow rate of 100 ml cm^{-3} at 540 °C (FeS-GRN5), (c) treatment for 15 hours in the 5 vol% of propane and 5 vol% of ammonia mixture in the flow of He at a total flow rate of 100 ml cm^{-3} at 540 °C (FeS-GRN15) and (d) treatment for 5 hours in the 30 vol% H_2O in helium at 600 °C (FeS-HT5) at a total flow rate of 45 ml min^{-1}. All the pretreatments were done in a quartz reactor, the same in which subsequently the catalytic activity was measured. Immediately after the activation the samples were calcined for 30 minutes in the flow of oxygen–helium mixture (5 vol% of oxygen) at 540 °C. In the case of the hydrothermal pretreatment, the temperature was decreased from 600 °C to 540 °C in the flow of helium, without calcination in the oxygen–helium mixture. All the pretreatments were done with 80 mg of the sample.

2.2 Characterization

The DR-UV-Vis spectra were measured using a UV-Vis spectrometer GBC CINTRA 303 equipped with a diffuse reflectance attachment with an integrating sphere coated with spectralon. Pure fumed silica was used as a reference material and samples were diluted with this silica (ratio 1 : 5) before measurements. Absorption intensity was expressed using Schuster–Kubelka–Munk equation.

EPR spectra of Fe^{3+} ions were monitored in the X-band region ($\nu \approx 9.4$ GHz) on the EPR spectrometer Miniscope MS 300. Spectra were recorded at room temperature and at 77 K using a finger dewar filled with liquid nitrogen, in the region of 50–450 mT. The magnetic field was measured with respect to the standard 4-hydroxy-2,2,6,6-tetramethylpiperidine-1-oxyl (TEMPOL).

FTIR spectra were recorded on a Nicolet 6700 FTIR spectrometer equipped with an MCT/A cryodetector, accumulating 64 scans at a spectral resolution of 2 cm^{-1}. Self-supporting pellets (*ca.* 10 mg cm^{-2}) were prepared from the sample powders and treated directly in a purpose-made IR cell allowing measurements at ambient and liquid nitrogen temperatures. The cell was connected to a vacuum pump allowing a residual pressure of $\sim 10^{-4}$ Torr.

XPS analyses were performed on a Kratos Axis Ultra spectrometer (Kratos Analytical, Manchester, UK) equipped with a monochromatized aluminium X-ray source (powered at 10 mA and 15 kV). The samples were fixed on a standard stainless steel multispecimen holder using a piece of double sided tape. The pressure in the analysis chamber was about 10^{-6} Pa. The angle between the normal to the sample surface and the direction of photoelectron collection was about 0°. Analysis was performed in the hybrid lens mode with the slot aperture, the resulting analyzed area was 700 μm × 300 μm. The pass energy was set at 160 eV for the survey scan and 40 eV for narrow scans. Under the latter conditions, the full width at half maximum (FWHM) of the Ag $3d_{5/2}$ peak of a standard silver sample was about 0.9 eV. Charge stabilization was achieved using the Kratos Axis device. The following sequence of spectra was recorded: survey spectrum, C 1s, O 1s, N 1s, Si 2p, Fe 2p and C 1s again to check for charge stability as a function of time and the absence of degradation of the sample during the analyses. The C–(C,H) component of the C 1s peak of carbon has been fixed at 284.8 eV to set the binding energy scale. Molar fractions were calculated using peak areas normalized on the basis of acquisition parameters after a linear background subtraction, experimental sensitivity factors and transmission factors were provided by the manufacturer.

2.3 Activity measurement

After the activation of the catalyst and the subsequent calcination in the flow of oxygen, the reaction mixture comprising 2.5 vol% of propane, 5 vol% of oxygen and 5 vol% of ammonia in helium at a total flow rate of 100 cm^3 min^{-1} was prepared. The reaction was carried out in a plug-flow fixed-bed reactor at atmospheric pressure, the reactor was made from quartz and the reaction was done with 80 mg of catalysts, (size of catalyst grains ranging from 0.25 to 0.50 mm) without the dilution of the catalyst. In the case of the isoconversion study Fe-silicalite was diluted with SiC in order to obtain the same volume of the catalytic bed (0.5 ml). The reaction was measured at a temperature of 540 °C. Analysis of the products was made in a TOS (time-on-stream) of 50 min. Product gases were analyzed online using GC (Agilent 7890) equipped with TCD and FID detectors. For the analysis of hydrocarbons (propane, propylene and ethane, ethene and methane) a HP PLOT/Q column was used. Permanent gases were analyzed on a HP molesieve column and nitriles were analyzed using a DB-WAX column. Conversion, selectivity and yields were calculated on the basis of the mass balance.

3. Results

3.1 UV-Vis spectroscopy

This spectroscopic technique is often used for the characterization of iron ions in the zeolite. The spectrum of the samples is ordinarily composed of two absorption regions, first one corresponding to Fe → O charge transfer (CT) bands (50 000–30 000 cm^{-1}) and second one corresponding to d–d transitions (30 000–17 000 cm^{-1}). Because these transitions are spin and symmetry forbidden, these signals are very weak and usually charge transfer bands are thus used for the description of the iron ion structure. UV-Vis spectra of hydrated diluted samples are shown in Fig. 1. The measured spectra were converted to Kubelka–Munk units. The spectrum of the fresh sample shows two well resolved bands, centered at 46 000 and 41 000 cm^{-1}.

Activation of the sample for 5 hours by GRN brings about significant structural changes, as represented in Fig. 1(B). There

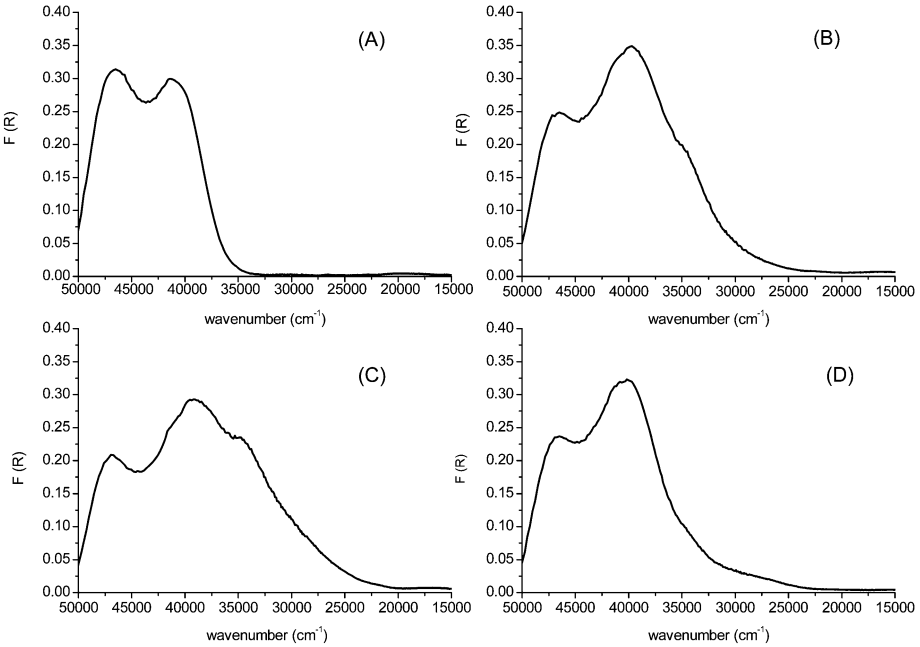

Fig. 1 UV-Vis spectra of hydrated Fe-silicalite, (A) FeS-calc3, (B) FeS-GRN5, (C) FeS-GRN15 and (D) FeS-HT5.

is a strong decrease of intensity of the bands at 46 000 cm^{-1}, and moreover the second CT maximum is shifted to a lower wavenumber (now being centered at 39 600 cm^{-1}), a similar feature is observed also for the samples FeS-GRN15 and FeS-HT5. All the activated samples are characterized by the absorption shoulder at about 35 000 cm^{-1}. The intensity of this band changes significantly depending on the sample, being the most intense for sample FeS-GRN15 and less intense for sample FeS-HT5. This shoulder is broadened to the lower wavenumber, namely to 25 000 cm^{-1} in the case of FeS-GRN5 and FeS-HT5, and to 20 000 cm^{-1} in the case of sample FeS-GRN15. In the case of sample FeS-HT5 we observe another band which is centered between 30 000 and 25 000 cm^{-1}.

Based on the confrontation of our spectra with data reported in the literature, it can be said that the fresh sample contains tetrahedrally coordinated iron incorporated into the framework of silicalite (absorption band at 46 000 and 41 000 cm^{-1}). In fact, it is usually reported that t_1–t_2 and t_1–e transitions involving Fe^{3+} in the FeO_4 tetrahedral group are responsible for two bands at 46 000 and 40 000 cm^{-1}.[28] The shift of the center of the absorption band from 41 000 to 39 000 cm^{-1} correlates well with the results described in the literature, where a similar shift was observed for the samples activated by calcination in air at high temperature.[28] These results suggest that upon the activation iron is extracted to extraframework positions, forming a different kind of coordination as indicated by the changes in the lower wavenumber. In order to highlight the changes in UV-Vis spectra of the samples upon the activation, the spectrum of the fresh calcined sample was subtracted from the spectra of activated samples; the resulting difference spectrum is reported in Fig. 2. In this figure it is well seen that there is a new negative band centered at 46 000 cm^{-1}, a new absorption band at a lower wavenumber of 35 000 cm^{-1}, and sample FeS-HT5 shows an absorption band below 30 000 cm^{-1} as was described above.

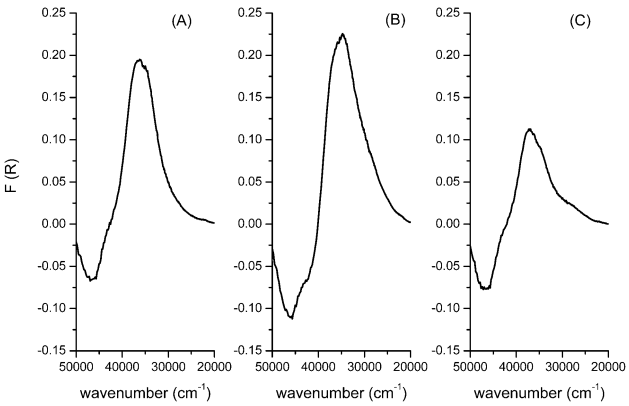

Fig. 2 UV-Vis difference spectra of activated samples, (A) FeS-GRN5, (B) FeS-GRN15 and (C) FeS-HT5.

The absorption band centered at about 35 000 cm^{-1} can be ascribed to square pyramidal[29] and distorted octahedra of isolated ions in extraframework positions as was observed in the case of iron on an alumina surface.[28] An absorption band between 30 000 and 25 000 cm^{-1} should be ascribed to octahedral Fe^{3+} ions in small oligonuclear clusters ($Fe^{3+}{}_xO_y$) inside zeolite pores.[16]

3.2 EPR spectroscopy

Although this spectroscopy has been used for characterization of iron sites in zeolites for a long time, still there is a discrepancy in the literature on the assignment of the individual signals to iron species. Fe^{3+} represents a paramagnetic system with $S = 5/2$ with spin Hamiltonian $\hat{H} = \mu_B gS + D\{S_z{}^2 - 1/3(S(S+1))\} + E(S_x{}^2 + S_y{}^2)$, where individual characters have their usual meanings,[30] D and E being zero-field splitting parameters describing the degree of

system distortion. It has been shown that in the case of the system containing iron ions in highly symmetric coordination, the EPR spectrum will be characterized by an isotropic signal at $g = 2$. In other cases, when coordination of iron is distorted, as is usually the case of iron doped zeolites, zero field splitting between the Kramers doublet will be large in comparison with the microwave frequency, and allowed EPR transitions will occur within the $m_s = \pm 1/2$ doublet giving rise to two following signals: (a) $g = 4.3$, in the case of strong rhombic distortion ($D \gg h\nu$, $D/E = 1/3$), (b) $g = 6$ if the system is characterized by axial distortion ($D \gg h\nu$, $E = 0$).[30]

From this very short summary of using EPR spectroscopy for characterization of Fe zeolites, it is evident that this technique cannot permit to draw a conclusion on the coordination of iron; rather it will give us the information only about the distortion of individual's coordination. This also emphasizes the fact that this spectroscopy serves only as a complementary technique for the characterization of iron. Moreover, as was pointed out by Fejes *et al.*,[31] pristine EPR spectra cannot be used to quantify iron ions in various distortions of coordination unless the EPR spectra are deconvoluted. On the basis of these prerequisites, we will use this characterization technique only as an additional source of the information of iron coordination, and we will not draw any conclusion on quantitative distribution of individual distortion of iron species.

The EPR spectra of the samples were recorded at the room temperature and at the temperature of liquid nitrogen. Spectra of the fresh samples together with the samples activated by GRN and HT are reported in Fig. 3.

The spectrum of the fresh, calcined Fe-silicalite recorded at 77 K is characterized by a very intense signal at $g = 4.3$, two signals at a lower field, $g = 5.3$ and 8.5, and a very weak signal at $g = 2$. The spectrum of the fresh sample recorded at 298 K shows the same signals, however their intensity change significantly. The most striking difference is the decreased intensity of the signal $g = 4.3$ thus following the Curie–Weiss law for the paramagnetic species. The same behavior is observed for other signals; however the change in intensity is not so strong. The spectrum of the sample activated for 5 hours by GRN recorded at 77 K is very similar to the fresh sample, the main difference is the decrease in intensity of the signal at $g = 4.3$ and broadening of the signal at $g = 2$. More pronounced are the changes in the spectrum at 298 K, where a very intense and broad signal at $g = 2$ is observed. An additional decrease of the intensity of the signal at $g = 4.3$ is observed for prolonged activation by GRN, in this case a well resolved signal is detected at $g = 6$. This pretreatment also brings about changes to the shape of the signal at $g = 2$ recorded at 77 K. As can be seen from the figure, there is another signal superimposed at $g = 2.1$. Activation by HT for 5 hours leads to very similar signal distribution: a signal at $g = 4.3$ loses its intensity upon increasing the temperature. Also in this case, the signal at $g = 2$ shows non-Curie behavior.

On the basis of the literature devoted to EPR of Fe zeolites, the signal at $g = 4.3$ in the fresh sample should originate from the middle Kramers doublet and could belong to tetrahedrally incorporated Fe^{3+}, in slightly rhombically distorted coordination (when $E/D = 1/3$),[32] most probably in the framework of zeolites. Although according to Fejes *et al.*,[33] this signal should originate from the extraframework species, taking into account the method of preparation from which we expect iron to be tetrahedrally coordinated and considering the results from UV-Vis spectroscopy and FTIR spectroscopy (see below) and also its Curie behaviour, we assign this signal to Fe ions in framework positions.

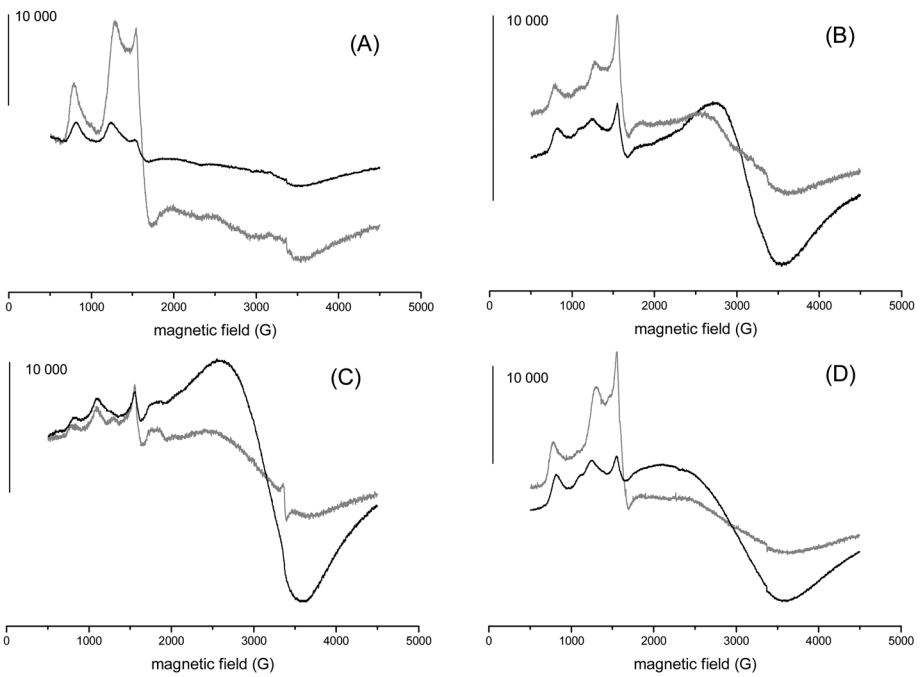

Fig. 3 EPR spectra of Fe-silicalite, measured at 77 K (grey line) and at 298 K (black line), (A) FeS-calc3, (B) FeS-GRN5, (C) FeS-GRN15 and (D) FeS-HT5.

The signal at $g = 4.3$ is usually accompanied by the signal at $g = 9$, in fact observed in the spectrum of the fresh sample (although in this case shifted to a slightly higher field), which is caused by rhombically distorted FeO_4 tetrahedra originating from the lowest Kramers doublet.[34] Attribution of the signal at $g = 5.5$ is not so unequivocal, in the literature there are different assignments of this signal, variously distorted tetrahedral coordination[35,36] or mononuclear Fe^{3+} in rhombically distorted tetrahedral coordination.[37] We will not attempt to assign this signal to any of these possible coordinations.

Spectra of the samples which were activated by HT and GRN show that the symmetry of the iron coordination is being changed depending on the method used. In the case of the activation by GRN for 5 hours compared to the fresh sample, the signal at $g = 2$ gains intensity at 77 K and 298 K, being more intense at RT. This non-Curie behavior unambiguously shows that this activation leads to formation of Fe_xO_y clusters. This assignment is in agreement with the literature where different kinds of high-temperature activation of iron doped zeolites led to formation of iron clusters.[7] Prolonged activation by GRN brings about very similar results, signals at $g = 6$ and at $g = 2$ become more intense. The signal at $g = 6$ very clearly observed in sample FeS-GRN15 and slightly in sample FeS-GRN5 could be ascribed to a less distorted tetrahedron which maintains C_{3v} axial symmetry (in this case $D \neq 0$, $E = 0$).[28] The signal at $g = 2$ of the sample activated for 15 h by GRN should also be attributed to the presence of the oxide clusters, considering its non-Curie behavior and also on the basis of the assignment of this peak in the case of the sample activated for 5 hours by GRN. The assignment of the very sharp, weak signal at $g = 2.1$, observed at 77 K, which is superimposed on the broad signal belonging to an oxide cluster of iron, is not so unambiguous (see that the shape of the spectrum at 77 K is quite similar to that of FeS-GRN5, however, the superimposed signal at $g = 2.1$ is not so well resolved). This signal is visible only at low temperature; at 298 K it cannot be detected thus it is indicative of paramagnetic behavior. In the literature this peak was observed in different cases, but only rarely commented.[38,39] This signal was attributed to coke radicals formed upon temperature treatment;[40] however we can rule out this possibility, because of the temperature behavior and also because of the history of the sample. Another assignment was[36] that the signal could be caused by superoxide ions (O_2^-), which are associated with iron ions. In other cases it was attributed to radical species formed upon the deposition of paramagnetic species O^- by N_2O,[11] which, however, is not our case. Most likely, by following the above assignment of the signal at $g = 6$, this superimposed signal could be attributed to the same species in accordance with the literature, where it has been ascribed to iron ions coordinated in a distorted tetrahedron maintaining C_{3v} axial symmetry. It was pointed out that the signal at $g = 2$ is not usually observed because of the line broadening.[28,41]

The spectrum of the sample activated by HT for 5 hours brings about very similar results as in the case of sample FeS-GRN5. We can suppose that the observed signals are caused by the same iron species as it was in the case of FeS-GRN5.

3.3 FTIR spectroscopy

Infrared spectra for the hydroxyl bands of the studied materials are shown in Fig. 4. Prior to the measurements, the samples were calcined at 450 °C under 80 mbar of oxygen overnight.

A fresh calcined sample shows absorption bands in the region of about 3730–3750 cm^{-1}, an absorption band centered at 3680 cm^{-1}, a broad absorption band centered at around 3500 cm^{-1} and another absorption band at 3632 cm^{-1}. Absorption bands in the region of 3730–3750 cm^{-1} belong to the silanol groups either at isolated positions or terminal SiOH groups in the hydrogen bonded silanol chains. An absorption band at 3680 cm^{-1} could be caused by the hydroxyl groups coordinated to extraframework iron atoms,[42] the third one (centered at 3500 cm^{-1}) belongs to the hydrogen-bonded silanol groups, so called hydroxyl nests, and the last band at 3632 cm^{-1} could be ascribed to the Brønsted acid site resulting from the hydroxyl groups between silicon and iron in the zeolite framework.[28] Characterization of fresh calcined samples confirmed that the sample contained iron in the framework positions (in accordance with UV-Vis spectroscopy) and moreover that calcination at 470 °C already caused formation of defect sites, as demonstrated by the presence of hydroxyl nests, which, as is known, are created upon the extraction of iron to extraframework positions.

Upon the activation there are some changes in the intensities of individual bands. Namely there is a decrease of intensity of the band at 3632 cm^{-1}, the decrease is most pronounced in the case of sample FeS-GRN15 in agreement with observation of a decrease in intensity of the EPR signal at $g = 4.3$ (see above). Another well observed change is a decrease in intensity of the band belonging to hydroxyl nests, the intensity decreases in the order FeS-GRN15 > FeS-GRN5 > HT5. These changes can be explained by condensation of the internal silanol groups with subsequent release of water, already observed by Bordiga *et al.*[28]

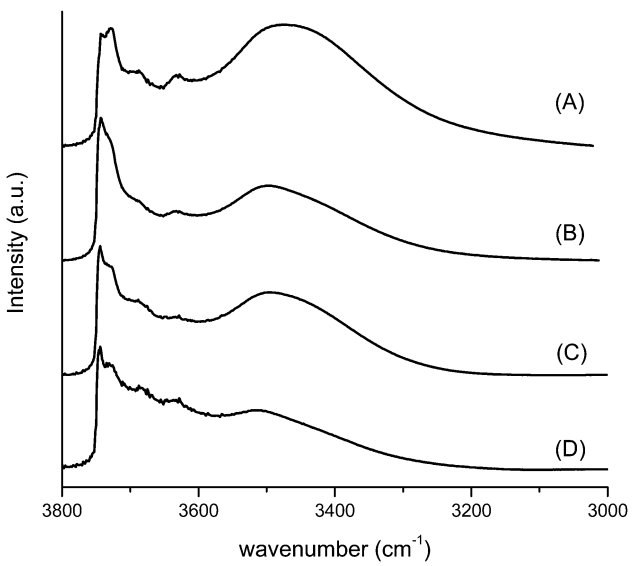

Fig. 4 FTIR spectra of Fe-silicalite, (A) FeS-calc3, (B) FeS-GRN5, (C) FeS-GRN15 and (D) FeS-HT5.

and Hensen *et al.*,[7] and also by further extraction of framework iron to extraframework positions leading to consecutive formation of these nests.

3.4 X-ray photoelectron spectroscopy

XPS measurements were performed on the fresh sample (FeS-calc3), on the sample activated for 5 hours by GRN (FeS-GRN5) and on the latter recovered after the catalytic test (FeS-GRN5-CT). Molar fractions are presented in Table 1. Following the synthesis, the measured surface Fe/Si ratio (~0.003) is lower than the expected one (0.0047) indicating that iron is probably embedded into the silicalite matrix. Moreover, this very low value leads to very poor spectra, avoiding any deeper analysis of the iron chemical state.

A trace amount of nitrogen was detected in the fresh sample. This can be explained by either remaining TPAOH from the synthesis and/or contamination. The level of N is very slightly increased after the GRN treatment. This could be seen as some nitrogen incorporation into the framework of the silicate but those two values remain in a too low range as compared to other nitridation processes done for which up to 1–2% of N can be incorporated at similar temperature but with much higher concentration of ammonia.[43,44] It is very likely that the calcination following the GRN treatment has induced the reversible process. The result of this would lead to a comparable surface composition for the fresh and GRN activated sample. However, this hypothetical nitridation followed by the calcination could have also induced some slight surface modifications, not evidenced by the XPS but able to explain the improvement in catalytic behavior of the GRN activated sample (see the results from the study of catalytic activity). After the catalytic test, no nitrogen was detected at the surface.

The content of carbon detected at the surface is twice higher in the case of the fresh sample when compared to the GRN sample. The sources of this carbon can come from the remaining template and the source of silica (TPAOH, TEOS), but also from the classical carbon contamination usually observed during XPS measurements. As all of the samples have been analyzed in the same times and under the same conditions, one can think that the level of the carbon contamination will remain to be more or less the same and then the supplementary content of carbon in the fresh sample can only be attributed to the remaining template. The calcination for 3 hours at 470 °C is then probably not sufficient to burn the template entirely. Binding energy of the Si 2p peak for the fresh sample was measured at 104.1 eV in respect of the position usually detected for silicate-like compounds.[45] Any shift towards the lower binding energies evidencing nitrogen incorporation[46] was not detected for the GRN activated sample before and after the catalytic test.

Table 1 XPS molar fractions of a fresh sample (FeS-calc3), of a GRN activated sample (FeS-GRN5) and of the latter recovered after the catalytic test (FeS-GRN5-CT)

	FeS-calc3	FeS-GRN5	FeS-GRN5-CT
Fe 2p	0.1	0.1	0.1
O 1s	51.6	56.2	55.2
N 1s	0.1	0.2	—
C 1s	14.8	6.8	7.0
Si 2p	33.5	36.7	37.8

3.5 Catalysis

The products of the direct ammoxidation of propane were acrylonitrile (ACN), propylene, acetonitrile (AcCN), carbon oxides and trace amounts of methane, ethane and ethene.

First we carried out the blank test with the purpose of confirming that no reaction in the gas phase can take place under our reaction conditions. We observed conversion of propane less than 1%, thus excluding the possibility that the results from the catalytic test could be influenced by reaction in the gas phase. Results from the study of the catalytic activity are shown in Fig. 5. Conversion of propane for the calcined sample is very low; being less than 5%, the prevalent product is propylene with almost 80% selectivity. The small conversion of propane corresponds to a small amount of extraframework iron ions in the calcined sample, as was evidenced using the UV-Vis and FTIR spectroscopies (see above). The high selectivity to propylene is most probably caused by the very low concentration of the active centers diluted by the zeolite matrix preventing overoxidation and by the presence of Brønsted acid sites (protons compensating for negative charge originate from framework iron) activating propane molecules.

Activation of the sample for 5 hours by GRN dramatically increases the conversion of propane to 24%, on the other hand the same time of pretreatment in the presence of water vapor leads only to 7% conversion. Activation of the Fe zeolite for 15 hours by GRN causes a slight increase of the conversion (28%) compared to a shorter time of the same pretreatment. Regarding the selectivities to ACN, the highest was obtained in the case of the sample activated for 5 hours by GRN (43%), longer activation by the same method led to lower selectivity (25%) which was caused mainly by the preferred formation of carbon oxides (see Fig. 5). These results can be explained by recalling the results from ESR and UV-Vis spectroscopy. There was higher concentration of oxide clusters as evidenced by a

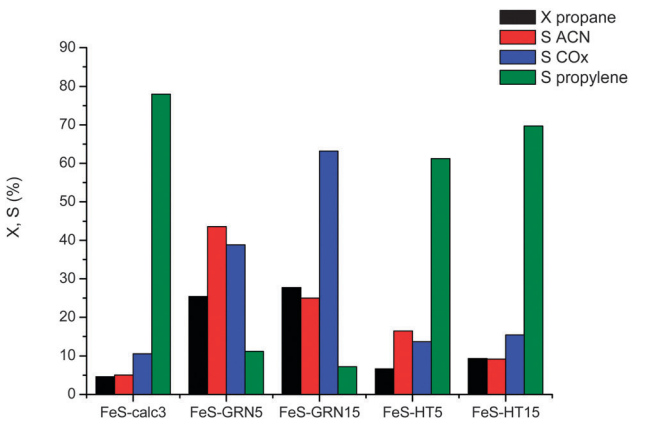

Fig. 5 Catalytic performance of Fe-silicalite activated using different methods in the direct ammoxidation of propane.

signal at $g = 2$ and broadening of the shoulders to 20 000 cm^{-1} in UV-Vis spectroscopy in the case of sample FeS-GRN15. The presence of these oxide clusters presumably caused oxidation of ACN to carbon oxides. The lowest selectivity to ACN was detected for the sample treated in the water vapor, being only 16%.

Yields of ACN follow the same trend as the selectivity to ACN, thus the highest being for sample FeS-GRN5 (10%), 15 hours of treatment resulted in the decline of the yield of *ca.* 30 rel%. In the case of hydrothermal pretreatment the yield was very low, hardly exceeding 1%. Comparing two different methods of activation, we see that better results are obtained on the sample which was pretreated by GRN.

In order to get deeper insight into the reaction we performed a study on the influence of contact time on the catalytic activity of Fe-silicalite which was activated for 5 hours by the GRN method as described in Experimental section (results are shown in Fig. 6). The amount of the catalyst loaded varied from 40 mg to 100 mg. Upon increasing the weight of the catalyst, conversion of propane increases almost linearly. The same graph shows also the dependence of the conversion of oxygen and ammonia on the amount of catalyst. See that the higher amount of Fe-silicalite (80 and 100 mg) leads to total conversion of oxygen, conversion of ammonia is about 85%. Fig. 7 reports the selectivity–conversion relationship of the same sample. Upon increasing conversion of propane selectivity to propylene gradually decreases, selectivity to acrylonitrile reaches its maximum already at 15% of conversion of propane, at higher conversion of propane selectivity to acrylonitrile decreases. This is caused by the lack of oxygen and ammonia as was shown in Fig. 6. Selectivity to carbon oxides progressively increases upon the increase of propane conversion, selectivity to cracking products and to acetonitrile does not show any specific dependence on conversion of propane, and their values are about 3% (cracking products) and 6% (AcCN).

These results also show that the reaction mechanism is quite complicated, including not only consecutive reaction

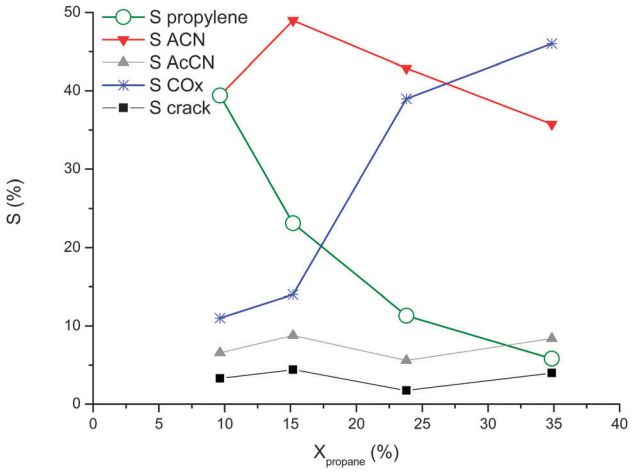

Fig. 7 Selectivity–conversion relationship of the FeS-GRN5 sample.

(dehydration of propane to propylene with subsequent formation of acrylonitrile) but also side reactions such as direct oxidation of propane to carbon oxides, cracking of propane and so on. Thus in order to properly compare the catalytic performance of samples activated for 5 hours, mainly the product distribution, it is necessary to perform an isoconversion study. For this purpose we changed the contact time (mass of the catalyst) to obtain the same conversion of propane. The results from this isoconversion study (conversion of propane 15%) are reported in Fig. 8. The figure clearly shows that samples activated by calcination, HT and GRN differ a lot concerning the product distribution and conversion of oxygen and ammonia. Both the conversion of oxygen and ammonia increase in the order calc < HT < GRN. More specifically, conversion of oxygen being as follows: 31%, 42% and 58%, conversion of ammonia being 30%, 48% and 67%. The selectivity to ACN increases in the order calc < HT < GRN. Selectivity to propylene follows the opposite trend (the highest being for the calcined sample). This shows that there is a pronounced difference in the activity of the samples, specifically in the velocity of the conversion of propylene to acrylonitrile. In the case of GRN activation, already

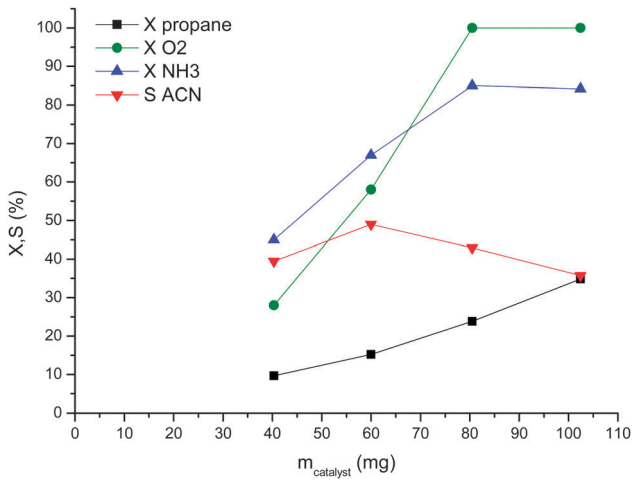

Fig. 6 Effect of amounts of catalyst loaded on FeS-GRN5 on catalytic performance.

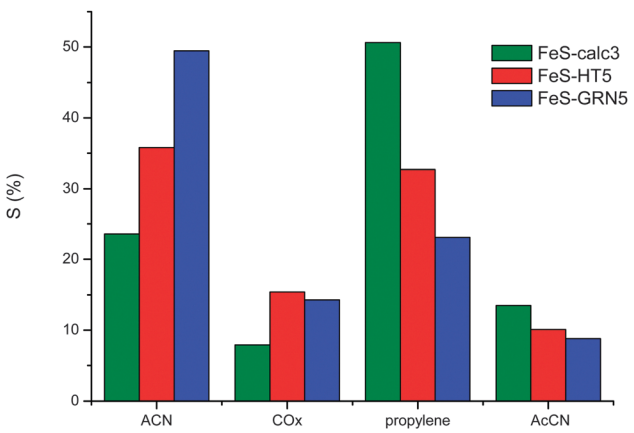

Fig. 8 Comparison of the product distribution of calcined and activated Fe-silicalite, conversion of propane = 15%.

at low conversion of propane (15%) the primary product of the ammoxidation of propane, propylene, is rapidly converted to ACN. Regarding the selectivities to carbon oxides of the samples activated by HT and by GRN for 5 hours we see that the sample pretreated by HT shows slightly higher selectivity to COx, compared to GRN. Worth mentioning are also selectivities to acetonitrile, which follow the same trend as selectivities to propylene (the highest for the calcined sample, the lowest for the nitrided sample). As is known from the literature,[24] acetonitrile can be formed by the decomposition of acrylonitrile which is caused by the presence of acidic protons. This could explain the highest selectivity to acetonitrile for the fresh calcined sample. In the case of this sample we expect to have the highest amount of iron in the framework position, thus to be a material with the highest concentration of Brønsted acid sites (see Fig. 4). Another possible way for creation of acetonitrile would be ammoxidation of ethene/ethane (originating from cracking of propane).

For better comparison of the activity of individual samples we calculated ''apparent TOF'', (apparent because we are referring to all iron cations presented in the zeolite, but we are fully aware of the fact that only the part of the iron contributes to the activity of the catalyst). Regarding the TOF, calculated for the mass of the catalyst we used for this isoconversion study, the highest TOF was obtained for sample FeS-GRN5, 207 h^{-1} and 122 h^{-1} were calculated for sample FeS-HT5 and only 65 h^{-1} for the calcined sample. This nicely shows the difference between the activities of the samples pretreated using various methods, emphasizing the high efficiency of gas-reduction nitridation.

4. Discussion

It is very interesting to compare the catalytic results with the results from spectroscopic studies. Starting from the fresh calcined sample, UV-Vis spectroscopy together with EPR and FTIR spectroscopy showed that iron was present mainly as the framework incorporated ion. However the sample also contained a small amount of extraframework iron atoms as was evidenced by an absorption band centered at 3680 cm^{-1} in FTIR spectra and by a very weak signal at $g = 2$ in EPR spectra. This distribution of iron did not lead to an active catalyst as is shown in Fig. 5. This corresponds well with earlier observed results from the study of catalytic activity of Fe-silicalite and Fe-ZSM-5,[11] where it has been shown that iron in the framework structure cannot contribute to catalytic activity.

The behavior of hydrothermally pretreated Fe-silicalite in the direct ammoxidation is very similar to that observed by Pérez-Ramírez *et al.*[23] and some of us[24] previously. In their study they reported the influence of individual oxidizing agents (O_2, N_2O, mixture of N_2O and O_2), and found out that direct ammoxidation of propane only in the presence of molecular oxygen brings about very poor results. In accordance with their study, we came to the same conclusion. On the other hand, pretreatment by GRN drastically improves the catalytic activity and also the selectivity to ACN in the ammoxidation of propane only with the molecular oxygen. The reason for this increased activity is however in the meantime not so clear.

Regarding the results from UV-Vis spectroscopy we observed that the main difference between the activation by GRN and by HT was in the case of hydrothermal pretreatment the presence of an absorption band centered between 30 000 and 25 000 cm^{-1} belonging to oligomeric clusters of Fe_xO_y. EPR spectroscopy was not very helpful in finding the differences between the individual pretreatments showing very similar signals for the samples. In both cases we observed signals belonging to clusters of Fe_xO_y, to tetrahedrally coordinated iron in distorted positions and also to iron ions in higher coordination.

Comparing the two samples FeS-GRN5 and FeS-HT5, we see that conversion of propane for sample FeS-GRN5 is almost 4 times higher compared to FeS-HT5. Also conversion of oxygen is much higher in the case of GRN (being almost 100% for the sample activated by GRN and about 30% for the sample activated by HT). Thus we see that the activity is caused by highly reactive species, which are not only able to rapidly convert propane but also cause high selectivity to acrylonitrile. If the activation by hydrothermal pretreatment and by GRN was done in the same manner, we would expect to see a similar result. The results from the isoconversion study also confirmed that the activated materials are highly different considering their selectivities.

As is well known from the literature, steam pretreatment serves very well for extraction of iron from framework to extraframework positions. Gas reduction nitridation is a novel method for activation of zeolite materials, which is very scarcely described in the literature. The most striking difference between these two activations is the fact that samples pretreated by HT need the presence of N_2O as the oxidizing agent in order to achieve good catalytic results. On the other hand GRN results in the active catalytic material which is able to catalyze the reaction only in the presence of oxygen. As was already proposed the enhanced activity would be caused by increased basicity of the material produced by insertion of nitrogen into the zeolite structure. Unfortunately, we were not able to detect any absorption band of any nitrogen species using FTIR spectroscopy. It is worth noting that in our previous work,[26] we were able to detect the absorption band belonging to $Si–NH_2$ and Si–NH–Si species, however in that case the nitridation was performed at higher temperature and in the flow of concentrated ammonia. Milder experimental conditions of nitridation (lower temperature and diluted stream of ammonia) would cause that very few nitrided species are created, hardly detectable using FTIR spectroscopy. The similar results were obtained using the XPS analysis, where we detected very low concentration of nitrogen in the activated sample compared to the fresh sample, and no trace of nitrogen for the activated sample after the catalytic test.

In order to further compare the two different activations, we performed the pretreatment of the sample in water vapor for prolonged time, for 15 hours, and characterized the sample using UV-Vis spectroscopy and also studied its activity in the ammoxidation of propane. The activity of this sample is shown

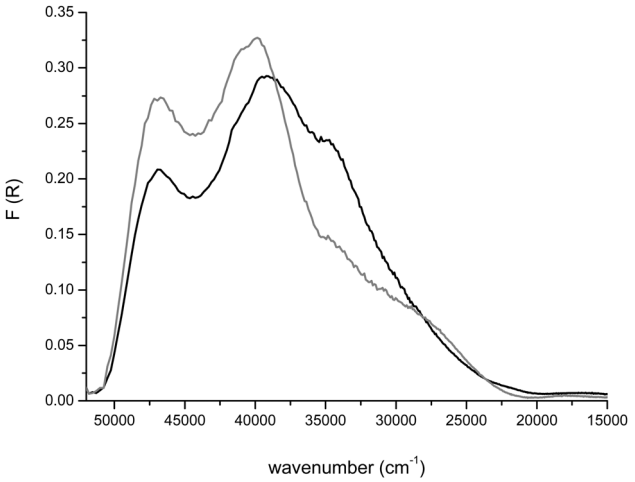

Fig. 9 Comparison of UV-Vis spectra of hydrated Fe-silicalite activated for 15 hours by HT (grey line) and by GRN (black line).

in Fig. 5. As it can be clearly seen such a long time did not improve results regarding the selectivity to ACN (being only 9%), conversion of propane little bit increased from 7 to 9%, leading to very poor yield (less than 1%). Comparison of UV-Vis spectra of the samples FeS-GRN15 and FeS-HT15 (Fig. 9) showed that HT activation does not lead to such a pronounced extraction of iron to extraframework positions compared to activation by GRN. This comparison led to another important observation (in accordance with previously stated assumption) that it seems to be the activation by HT and by GRN leads to different distribution of iron after its extraction from the framework. See that the absorption band at 35 000 cm^{-1} is much more intense for sample FeS-GRN15 compared to FeS-HT15, which is very similar to the comparison between the samples FeS-HT5 and FeS-GRN5. On the other hand, the absorption band below 30 000 cm^{-1} is more pronounced in the case of FeS-HT15 (again, likewise for the samples FeS-HT5 and FeS-GRN5). This signifies that upon the activation by HT and by GRN we obtain two different samples, which vary a lot regarding their catalytic performance and iron distribution.

5. Conclusions

In our study we attempted to compare the catalytic performance of the samples activated by two different methods: hydrothermal activation and gas-reduction nitridation and by means of the different characterization techniques (UV-Vis, FTIR, EPR and X-ray Photoelectron Spectroscopy) reveal the changes in the structure of Fe-silicalite. Our results can be summarized as follows:

(i) Upon the activation of Fe-silicalite by hydrothermal pretreatment and by GRN pretreatment we obtain two different samples, which differ regarding their catalytic performance and also coordination of extracted iron.

(ii) Activation in the diluted stream of ammonia and propane resulted in the more active catalyst, which also showed higher selectivity to acrylonitrile. This was caused most probably by the rapid conversion of formed propylene to acrylonitrile.

(iii) GRN activation for 5 hours does not lead to such a pronounced formation of iron oxide particles, which has a positive effect on the catalyst performance, on the other hand activation in the steam led to formation of Fe_xO_y clusters, which negatively influenced the catalyst behavior.

(iv) It is very hard to extract all iron ions from framework sites to extraframework positions as was shown in the case of the sample activated for 15 hours by GRN. Compared to GRN, extraction of iron from framework positions in the steam was slower as evidenced using UV-Vis spectroscopy.

Acknowledgements

The financial support of the Grant Agency of the Czech Republic under the project Nos. P106/12/P083 (KR) and P106/12/G015 (RB) and the UniCRE project (CZ.1.05/2.1.00/03.0071) (EB) are highly acknowledged.

References

1 J. Pérez-Ramírez and A. Gallardo-Llamas, *J. Catal.*, 2004, **223**, 382.
2 E. V. Kondratenko and J. Pérez-Ramírez, *Appl. Catal., A*, 2004, **267**, 181.
3 J. Pérez-Ramírez and A. Gallardo-Llamas, *Appl. Catal., A*, 2005, **279**, 117.
4 A. S. Kharitonov, G. A. Sheveleva, G. I. Panov, V. I. Sobolev, Y. A. Paukshtis and V. N. Romannikov, *Appl. Catal., A*, 1993, **98**, 33.
5 J. B. Taboada, E. J. M. Hensen, I. W. C. E. Arends, G. Mul and A. R. Overweg, *Catal. Today*, 2005, **110**, 221.
6 E. J. M. Hensen, G. Zhu, P.-H. Liu, K.-J. Chao and R. A. van Santen, *J. Catal.*, 2004, **226**, 466.
7 E. J. M. Hensen, Q. Zhu, R. A. J. Janssen, P. C. M. M. Magusin, P. J. Kooyman and R. A. van Santen, *J. Catal.*, 2005, **233**, 123.
8 E. J. M. Hensen, Q. Zhu and R. A. van Santen, *J. Catal.*, 2005, **233**, 136.
9 V. I. Sobolev, K. A. Dubkov, E. A. Paukshtis, L. V. Pirutko, M. A. Rodkin, A. S. Kharitonov and G. I. Panov, *Appl. Catal., A*, 1996, **141**, 185.
10 M. A. G. Hevia and J. Pérez-Ramírez, *Appl. Catal., B*, 2008, **77**, 248.
11 J. Pérez-Ramírez, M. S. Kumar and A. Brückner, *J. Catal.*, 2004, **223**, 13.
12 M. N. Debbagh, C. Salinas Martínez de Lecea and J. Pérez-Ramírez, *Appl. Catal., B*, 2007, **70**, 335.
13 J. Pérez-Ramírez, F. Kapteijn and A. Brückner, *J. Catal.*, 2003, **218**, 234.
14 M. Schwidder, M. S. Kumar, U. Bentrup, J. Perez-Ramirez, A. Brückner and W. Grünert, *Microporous Mesoporous Mater.*, 2008, **111**, 124.
15 M. Schwidder, M. S. Kumar, A. Brückner and W. Grünert, *Chem. Commun.*, 2005, 805.

16 M. Schwidder, M. S. Kumar, K. Klementiev, M. M. Pohl, A. Brückner and W. Grünert, *J. Catal.*, 2005, **231**, 314.
17 X. Feng and W. K. Hall, *J. Catal.*, 1997, **166**, 368.
18 A.-Z. Ma and W. Grünert, *Chem. Commun.*, 1999, **71**.
19 J. Pérez-Ramírez, *J. Catal.*, 2004, **227**, 512.
20 J. Pérez-Ramírez, F. Kapteijn, J. C. Groen, A. Domenech, G. Mul and J. A. Moulijn, *J. Catal.*, 2003, **214**, 33.
21 E. V. Kondratenko and J. Pérez-Ramírez, *Catal. Today*, 2007, **121**, 197.
22 J. Pérez-Ramírez, J. C. Groen, A. Brückner, M. S. Kumar, U. Bentrup, M. N. Debbagh and L. A. Villaescusa, *J. Catal.*, 2005, **232**, 318.
23 J. Pérez-Ramírez, N. Blangenois and P. Ruiz, *Catal. Lett.*, 2005, **104**, 163.
24 R. Bulanek and F. Castek, *Top. Catal.*, 2007, **45**, 233.
25 R. Bulanek, K. Raabova and E. Badurova, *Catal. Today*, 2012, **179**, 73.
26 K. Raabova, R. Bulanek and E. Badurova, *Catal. Today*, 2013, **204**, 54.
27 A. Zecchina, M. Rivallan, G. Berlier, C. Lamberti and G. Ricchiardi, *Phys. Chem. Chem. Phys.*, 2007, **9**, 3483.
28 S. Bordiga, R. Buzzoni, F. Geobaldo, C. Lamberti, E. Giamello, A. Zecchina, G. Leofanti, G. Petrini, G. Tozzolo and G. Vlaic, *J. Catal.*, 1996, **158**, 486.
29 G. Centi, S. Perathoner, F. Pino, R. Strigo, G. Giordano, A. Katovic and V. Pedulà, *Catal. Today*, 2005, **110**, 211.
30 A. Bruckner, *Adv. Catal.*, 2007, **51**, 265.
31 P. Fejes, K. Lázár, I. Marsi, A. Rockenbauer, L. Korecz, J. B. Nagy, S. Perathoner and G. Centi, *Appl. Catal., A*, 2003, **252**, 75.
32 D. Goldfarb, M. Bernardo, K. G. Strohmaier, D. E. W. Vaughan and H. Thomann, *J. Am. Chem. Soc.*, 1994, **116**, 6344.
33 P. Fejes, I. Kiricsi, K. Lázár, I. Marsi, A. Rockenbauer, L. Korecz, J. B Nagy, R. Aiellof and F. Testa, *Appl. Catal., A*, 2003, **242**, 247.
34 A. Tuel, I. Arcon and J. M. M. Millet, *J. Chem. Soc., Faraday Trans.*, 1998, **94**, 3501.
35 A. V. Kucherov, C. N. Montreuil, T. N. Kucherova and M. Shelef, *Catal. Lett.*, 1998, **56**, 173.
36 H.-Y. Chen, E.-M. El-Malki, X. Wang, R. A. van Santen and W. M. H. Sachtler, *J. Mol. Catal. A: Chem.*, 2000, **162**, 159.
37 D. Meloni, R. Monaci, V. Solinas, G. Berlier, S. Bordiga, I. Rossetti, C. Oliva and L. Forni, *J. Catal.*, 2003, **214**, 169.
38 A. V. Kucherov and M. Shelef, *J. Catal.*, 2000, **195**, 106.
39 B. Gil and A. Adamski, *Microporous Mesoporous Mater.*, 2010, **127**, 82.
40 A. Bruckner, U. Lohse and H. Mehner, *Microporous Mesoporous Mater.*, 1998, **20**, 207.
41 T. Castner, G. S. Newell, W. C. Holton and C. P. Slichter, *J. Chem. Phys.*, 1960, **32**, 668.
42 A. Zecchina, F. Geobaldo, C. Lamberti, S. Bordiga, G. Turnes Palomino and C. Otero Arean, *Catal. Lett.*, 1996, **42**, 25.
43 M. Srasra, S. Delsarte and E. M. Gaigneaux, *J. Phys. Chem. C*, 2010, **114**, 4527.
44 K. Narasimharao, M. Hartmann, H. H. Thiel and S. Ernst, *Microporous Mesoporous Mater.*, 2006, **90**, 377.
45 Y. Zhao, Y. Qi, Y. Wei, Y. Zhang, S. Zhang, Y. Yang and Z. Liu, *Microporous Mesoporous Mater.*, 2008, **111**, 300.
46 Y. Xia and R. Mokaya, *J. Mater. Chem.*, 2004, **14**, 2507.